Bandgap Engineering and Plasmonically Enhanced Sun Light Photocatalyis in Au/$Cd_{1-x}Zn_xS$ Nanocomposites

Pavan Prasad Gotipamul
SRM Institute of Science and Technology
Karthik Dilly Rajan
SRMIST: SRM Institute of Science and Technology
Shweta Khanna
SRMIST: SRM Institute of Science and Technology
Maheswaran Rathinam
SRMIST: SRM Institute of Science and Technology
Chidambaram Siva (sivac@srmist.edu.in)
SRM University https://orcid.org/0000-0001-5088-4869

Research Article

Keywords: CdZnS, Sun light, Photocatalyst, Band gap engineering, Plasmonic, SILAR

Posted Date: February 8th, 2021

DOI: https://doi.org/10.21203/rs.3.rs-167826/v1

Abstract

Metal nanoparticles incorporated semiconductor nanomaterials generally holds a series of advantages especially enhanced electron-hole pair lifetime and thus exhibits superior solar energy conversions. In this study, we report a facile solution processing of Au incorporated $Cd_{1-x}Zn_xS$, where x = 0, 0.25, 0.5, 0.75 & 1, nanocomposites and their enhanced photocatalytic applications. The Au/CdZnS nanocomposites were investigated for their structural, morphological, optical and photocatalytic properties. The XRD patterns indicated the crystalline sizes of CdZnS are found to fall with the range of 1-3 nm. The electron microscopic images publicized the average particle size of $Cd_{0.25}Zn_{0.75}S$ is 4 nm. The bandgap values of pristine CdS, pristine ZnS, $Cd_{0.75}Zn_{0.25}S$, $Cd_{0.5}Zn_{0.5}S$ and $Cd_{0.25}Zn_{0.75}S$ are 2.21 eV, 3.4 eV, 2.29 eV, 2.31 eV and 2.53 eV, respectively. The optical band gap of the CdZnS nanomaterials have got reduced for Au incorporation due to the occurrence of red shift and the enhanced visible region absorption for the inclusion of Au. The visible light photocatalytic effect of the nanocomposites have been evaluated with methylene blue (MB) dye degradation reaction under sunlight light exposure. The Au incorporated $Cd_{0.25}Zn_{0.75}S$ nanocompound had exhibited 97 % of photocatalytic degradation of MB dye molecules which is 20% higher than the bare $Cd_{0.25}Zn_{0.75}S$ nanocompound.

Introduction

The photo-assisted catalytic decomposition or fragmentation of organic pollutants employing visible light semiconductors have been recognized as promising methodology for efficient removal of pollutants. Amongst the semiconductors endeavoured for efficient photocatalysis of pollutant removals, metal sulfides are considered to be the most preferable materials. CdS is one of the widely studied photocatalysts possess suitable band gap of 2.4 eV and appropriate energy band positions for photocatalytic reactions [1]. Nevertheless, low activity and stability of pure CdS and self photocorrosion strongly and toxicity issue limits from its practical application. In order to overcome this shortcoming, combining CdS with other metal sulfides or incorporation of metal particles is extremely feasible fashion [2]. Meanwhile the band edge positions of CdS are comparatively lower than that of certain materials such as ZnS. Incorporating ZnS in CdS systems, resulting $Cd_{1-x}Zn_xS$ nanocompounds could substantially elevate the energy level positions in which high efficiency could be achieved. Besides ZnS possess excellent charge transport properties, high electron mobility, better thermal stability, large exciton binding energy (40 meV) and as wide band gap on par to CdS which generally improve photoabsorption properties [3].

Making of $Cd_{1-x}Zn_xS$ solid solution is a powerful strategy for improved photocatalytic activity compared to their pristine counterparts either CdS or ZnS [4, 5], in which recombination of photogenerated charge carriers is the major drawback. The recombination can be further avoided abruptly via incorporating the plasmonic metal nanoparticles, such as Ag, Au, Pt, and Pd on the surface of the $Cd_{1-x}Zn_xS$ nanomaterials [6, 7]. These plasmonic metal nanoparticles inhibit the electron hole pair recombination by acting as electron trap and also enhance the incident photon absorbance by its localized surface

plasmon resonance (LSPR) properties. Since, the studies on various methodologies on incorporation of various metal nanoparticles on CdZnS deserves more advantages.

Considering the above-mentioned parameters, we have synthesized Au incorporated $Cd_{1-x}Zn_xS$ with X = 0 to 1. Band gap of the $Cd_{1-x}Zn_xS$ tune by varying composition of Cd^{2+} and Zn^{2+}. The activity of $Cd_{1-x}Zn_xS$ in photocatalytic dye degradation is much higher than bare CdS and ZnS, the most active photocatalyst in the $Cd_{1-x}Zn_xS$ series is $Cd_{0.25}Zn_{0.75}S$ and Au/ $Cd_{0.25}Zn_{0.75}S$.

Experimental Section

Materials:

Chemical reagents used in production of $Au/Cd_xZn_{1-x}S$ photocatalyst are analytical grade. Cadmium acetate dehydrate (Cd $(CH_3COO)_2.2H_2O$), zinc acetate dehydrate (Zn $(CH_3COO)_2.2H_2O$), sodium sulfide (Na_2S), auric chloride (HAuCl4), sodium borohydride ($NaBH_4$) and methylene blue were purchased from SRL Pvt. Chemicals, India. The purchased chemicals were used without any further purification.

Materials Synthesis of Au decorated $Cd_{1-x}Zn_xS$

We have followed co-precipitation methodology for the preparation of $Cd_{1-x}Zn_xS$ solid solution followed by the incorporation of Au nanoparticles via ultrasonication assisted SILAR (successive ionic layer adsorption and reaction) technique. In a typical synthesis of $Cd_{1-x}Zn_xS$ (X = 0, 0.25, 0.5, 0.75 & 1), given quantity of Cd $(CH_3COO)_2.2H_2O$ and Zn $(CH_3COO)_2.2H_2O$ in different molar ratio of Cd^{2+}/Zn^{2+} were mixed well in 100 ml of water. Further sodium sulfide solution (0.1 M in 100 mL water) was added drop wise under vigorous stirring condition at room temperature. After complete reaction, we have filtered the precipitates and washed several times with water and ethanol. The obtained materials were dried at 80°C for 12h in hot air oven.

The obtained metal sulphide nanoparticles of 0.1 g were dispersed in Au^{3+} solution (0.0016 g of $HAuCl_4$ in 60 ml H_2O). Under ultrasonication and manual stirring condition we have further added an appropriate amount of sodium borohydride ($NaBH_4$) solution (3g $NaBH_4$ in 300 ml) till change in the colour become constant. The composite materials were collected via centrifuge and washed for several times. Further the samples were dried at 80°C for 12 h in hot air oven after washing. Thus, obtained materials were further utilized directly for the characterization and sunlight photocatalytic studies without any further processing.

Materials characterization

Crystal structure of the as-prepared photocatalyst was identified by PXRD (powdered X-ray diffractometer) by using PANalytical's X'pert pro with Cu Kα radiation (λ=1.5405 A°) in the 2θ range from 20° to 80°. The optical absorption properties were studied using shimadzu (UV-3600) spectrometer with

the absorption wavelength range 200 to 800 nm. The surface morphology and elemental composition of the photocatalyst were analysed by field- emission scanning electron microscopy (FE-SEM) FEI Nova Nano-SEM operating at 15kv, attached with energy dispersive X-ray spectrometer. High-resolution transmission electron microscopic images (HR-TEM) were captured with a JEOL JEM-2010 (Japan) operated at 200 kv.

Sun light photocatalytic Studies

Photocatalytic activity of the obtained specimens was estimated by the degradation of methylene blue (MB) under the direct sunlight illumination. A typical test was carried out using 50 mg of as prepared photocatalyst nanomaterials and 50 ml of (10mg/L) MB dye solution. Firstly, the mixture was stirred magnetically in dark condition for 30 min in order to achieve absorption, adsorption and desorption equilibrium between nanomaterials and dye molecules. At every certain time interval, 3 ml of dye solution was collected after placed under bright sunlight and centrifuged to remove the catalysts. The concentration of the resultant dye in the solution was estimated by measuring the absorbance at the maximum absorption wavelength (λ = 664 nm) of MB using UV-vis spectrometer. The photodegradation percentage of the MB dye was calculated by the following equation:

Degradation (%) = $(C_0 - C_t)/C_0 \times 100$, where, C_0 is initial concentration and C_t is time interval

Result And Discussions

Structural studies:

The structural properties of $Au/Cd_{1-x}Zn_xS$ nanocomposites were analysed using XRD technique. All the patterns (Fig. 1) were exhibited broader peaks with high full width at half maximum (FWHM) indicating the small crystalline structured formed in all the samples via the conducted synthesis protocol. The pattern of pristine CdS nanoparticles exhibited three peaks at the 2θ positions 26.38°, 43.7° and 51.6° are representing the planes (111), (220) and (311), respectively in accordance to the JCPDS card # 75–0581 of cubic crystal system. For introducing the Zn^{2+} ions in the CdS system, the peak positions have shifted towards higher 2θ positions depend upon the concentration of Zn^{2+} [8, 9]. The pattern of pristine ZnS has exhibited the 3 peaks in the 2θ positions 28.80°, 47.83° and 56.62° representing the (111), (220), (311) planes, respectively in accordance to the JCPDS card # 77-2100 (cubic crystal system). The peak position shift for Zn^{2+} could be attributed to the relatively smaller ionic radii of Zn^{2+} (0.74A°) than the Cd^{2+} (0.97A°) [5]. The successive shift in the peak positions and absence of any other peaks corresponding to CdS or ZnS present in the CdZnS nanoparticles indicate the purity of the specimens and the avoidance of composite structures. This could be attributed to comparable electronegativity values of Zn (1.6) and Cd (1.7) atom [10]. The patterns of the Au/CdZnS indicated the crystalline peaks at 38° corresponding to (111) peak [11, 12].

We have calculated the crystallite size of the synthesized materials from the XRD data using Debye - Scherrer formula, **$D = K\lambda/\beta\cos\theta$,** where, D is crystalline size, K is a constant related to particle morphology typically 0.9 for spherical particles, λ is the wavelength of X-ray (0.1542 nm), β full width of half maximum intensity (FWHM) of diffraction peak, θ is centre position of Bragg's angle [13]. We have also calculated the lattice constant value (a) as **$a = d(h^2 + k^2 + l^2)^{1/2}$**, where $d = n\lambda/2\sin\theta$, n is the order of diffraction and (h k l) are the miller indices. Further we have also evaluated the lattice parameter values of the $Cd_xZn_{1-x}S$ and the graphs shown the linear decrease in the lattice constant values for the addition of Zn^{2+} ions.[14].

Morphological analysis:

The scanning electron micrographs (SEM) plays an effective role in the study of surface morphology of the nanomaterials. Figure 3(a-e) represent the SEM images of pristine and compound specimens ($Cd_{1-x}Zn_xS$). From the SEM images particle morphology of the materials retained in all the cases are identified. The images explicated the agglomerated nanoparticles. This agglomeration could be reasoned to many factors such as reaction rate, pH, impurity, surface energy, particle charges and product constant for solubility [15, 16, 17]. The SEM images of Au incorporated $Cd_{1-x}Zn_xS$ nanoparticles are shown in Fig. 3(f-j). The SEM images indicated the unaltered morphology in the $Cd_xZn_{1-x}S$ specimens for Au incorporation.

Transmission electron microscopic images obtained for the $Cd_{0.25}Zn_{0.75}S$ nanocompound (Fig. 4a&b) & Au/ $Cd_{0.25}Zn_{0.75}S$ nanocomposites (Fig. 4c&d) have exhibited the particulate morphology of the obtained nanocomposites. The images indicated the size of the particles falls in between 3 nm to 5 nm and their average particle size was calculated to be $Cd_{0.25}Zn_{0.75}S$ is 4 nm. The TEM images also reveal the particles possessing identical dimensions and are aggregated to each other. The concentration of Au on par to the CdZnS is quite low in the composites, since that TEM images of Au/ $Cd_{0.25}Zn_{0.75}S$ are also mainly showcase the $Cd_{0.25}Zn_{0.75}S$ nanoparticles rather the Au nanoparticles [18]. Figure 4(b&d) shows the lattice fringes with d-spacing of 0.32 nm & 0.33 nm could be assigned to the (111) lattice plane of zinc blend CdZnS & Au/CdZnS. The EDS spectrum is a tool to explore the chemical composition present in the nanocomposites. The EDS spectrum of $Cd_{0.25}Zn_{0.75}S$ and Au/$Cd_{0.25}Zn_{0.75}S$ were shown in Fig. 5., which confirm the existence of the elements Cd, Zn, S & Au in the corresponding specimens.

UV-visible absorption spectroscopy

We have obtained UV–vis absorption spectrum of the Au incorporated $Cd_{1-x}Zn_xS$ nanoparticles to study the energy band positions and electronic transitions and are plotted as given in Fig. 6&7(a& b). The absorption edge of various CdZnS depends on the compositions of Cd^{2+} & Zn^{2+} ions, and lies within the values of ZnS (375 nm) and CdS (594 nm) band edge positions. The spectrum of pure ZnS shown the strong absorption of UV region photons and the absorption maximum at ~ 320 nm, whereas the absorption maximum of CdS falls in visible region with absorption maximum at ~ 500 nm. UV–vis absorption measurement is a convenient and effective method for investigating the band structures of

photocatalyst **[26]**. The band gap of the $Cd_{1-x}Zn_xS$ can be estimated by tauc plot of $(\alpha h\upsilon)^2$ vs $(h\upsilon)$, where, α is the absorption coefficient and hυ is the photon energy. Thus, calculated bandgap value of pristine ZnS is 3.44 eV and CdS is 2.21 eV. The band gap value of bulk ZnS generally could be observed from 3.56 eV to 3.764 eV, and the bulk CdS exhibits at 2.4 eV [20]. Relatively reduced bandgap value of these nanomaterials compared to the bulk counterparts could be assigned to the materials formed at nanoscale. For the introduction of Zn^{2+} ions in CdS nanocompound resulted in significant blueshift in the band edge position have been observed and this further increased for increasing the concentration of Zn^{2+} ions. The calculated bandgap values of $Cd_{0.75}Zn_{0.25}S$, $Cd_{0.5}Zn_{0.5}S$, and $Cd_{0.25}Zn_{0.75}S$ are 2.29 eV, 2.31 eV and 2.55 eV, respectively. The received high variation in bandgap value and less linearity in its change for high Zn^{2+} ions are well matching with the existing literature [21]. The spectrum obtained for the Au incorporated CdZnS nanocomposites have shown enhanced absorption in the visible region than their pristine counterparts.

Figure 8. The position of the conduction band minimum and valance band maximum can be calculated by electronegativity equations, $E_{CB} = \chi - E_e - 0.5E_g$ and $E_{VB} = E_{CB} + E_g$, where, E_{CB} denotes conduction band potential, E_{VB} is valence band potential, E_g band gap of the photocatalyst, χ absolute electronegativity of constituent atom Cd (4.3), Zn (4.45), S (6.62), E_e represents the energy of free electron in hydrogen scale (4.5eV) [27,28]. The position of conduction band and valence band of $Cd_{1-x}Zn_xS$ were shifted more negative potential and more positive potential with increasing X value as shown in fig [22].

Sunlight photocatalytic activity

Photocatalytic activity of the attained nanocomposites was estimated by measuring degradation of MB in aqueous solution under sun light exposure. The degradation of MB dye molecules was estimated via the absorption intensity at 664 nm of the dye solution at serious of intervals. Based on the absorption intensity we have evaluated the C/C_0 values for all the samples. The graph plotted for C/C_0 versus time intervals illustrated the degradation rate of the dye molecules for various catalysts (Fig. 9a). Initially, pristine CdS nanoparticles have exhibited the photocatalytic percentage of degradation is about 49 % for 150 min. Further, the graph depicted the enhanced efficiency obtained for the CdZnS nanocomposites on par to the pristine CdS and ZnS. The percentage of degradation of MB dye molecules for the catalysts, $Cd_{0.75}Zn_{0.25}S$, $Cd_{0.5}Zn_{0.5}S$, $Cd_{0.25}Zn_{0.75}S$ and ZnS are 62%, 70%, 77.6% and 69.5% respectively. Very low degradation efficiency of CdS over the other Zn^{2+} presented materials could be reasoned to the relatively lower conduction band position of Cd^{2+} leading to easy photocorrosion. The incorporation of Zn^{2+} in the CdS elevate the conduction band position to more negative values since the conduction position of ZnS is higher than the conduction band position of CdS. ZnS have possessed only 69.5% of degradation due to its wideband gap nature. We have attained the highest efficiency of 77.65 % of degradation for $Cd_{0.25}Zn_{0.75}S$ nanocompound, in which 75 % of Zn^{2+} were utilized.

Immense increase in the efficiency of the Au incorporated nanomaterials were realized in the conducted photocatalytic reactions under sunlight. Addition of Au nanoparticles in CdZnS nanocompounds greatly

improved the photocatalytic activity through LSPR properties [23]. Plasmonic properties of the Au nanoparticles intensifies the optical absorption of $Cd_xZn_{1-x}S$ directing to generation of more excitons. The Au/$Cd_{0.25}Zn_{0.75}S$ photocatalyst exhibited highest photocatalytic activity towards the MB degradation. The photocatalytic degradation of Au incorporated $Cd_{0.25}Zn_{0.75}S$ was achieved to 97% of degradation, which is 20% higher than the $Cd_{0.25}Zn_{0.75}S$. The percentage of degradation of other Au incorporated specimens of CdS, $Cd_{0.75}Zn_{0.25}S$, $Cd_{0.5}Zn_{0.5}S$ and ZnS are respectively 93.75%, 91.5%, 93% and 94%. Thus, enhanced photocatalytic activity in CdZnS materials were achieved through the involvement of trivial loading of Au on $Cd_{0.25}Zn_{0.75}S$ nanoparticles.

Charge transfer mechanism

Figure 9. To understand photoinduced charge transfer mechanism in the Au/$Cd_{0.25}Zn_{0.75}S$, we have plotted the energy band diagram based on the obtained results in the optical spectroscopic studies. The fermi level of Au was located at + 0.5 V versus NHE and conduction band of the $Cd_{0.25}Zn_{0.75}S$ located at -0.45 V versus NHE. Upon the irradiation of the visible photons the excited electron from conduction band of $Cd_{0.25}Zn_{0.75}S$ transferred to the Au due to this energy difference. Thus, Au nanoparticles trap the electrons from the conduction band of CdZnS by acting as electron sink and diminish the electron-hole recombination process. The transferred electrons in the Au nanoparticles reacts with oxygen molecules adsorbed on the surface of the catalyst to form superoxide radicals ($O_2^{\cdot}$). Meanwhile the holes in valance band react with water and produce OH. radicals. These active radicals further conduct the efficient degradation process.

Conclusions

In this study, Au/$Cd_{1-x}Zn_xS$ nanocomposite with X = 0, 0.25, 0.5, 0.75 & 1 were synthesized by simple co-precipitation technique followed by SILAR. The obtained X-ray diffraction patterns indicated the phase purity of the obtained materials. The lattice parameters of CdZnS nanocomposites have got linear change for the linear change in the chemical compositions. The TEM images indicated the particle size of CdZnS falls in the range of 3–5 nm. The UV-vis absorption spectra indicated the Au incorporation enhanced visible region photons absorption in CdZnS nanocompounds. Further conducted photocatalytic investigations revealed the enhanced efficiency in MB dye degradation for Au incorporation in CdZnS nanocomposite. Our studies suggest the plasmonic Au incorporated $Cd_{0.25}Zn_{0.75}S$ photocatalyst possess the superior photocatalysis on par to the pristine ZnS and CdS nanomaterials under sunlight.

References

1. L.Wang, Z. Liu, J. Han, R. Li and M. Huang, Stepwise Synthesis of Au@CdS-CdS Nanoflowers and Their Enhanced Photocatalytic Properties. J. Nanoscale Res. Lett. 14:148 (2019).
2. H. Wang, Y. Li, D. Shu, X. Chen, X. Liu, X. Wang, J. Zhang and H. Wang, CoPtx-loaded Zn0.5Cd0.5S nanocomposites for enhanced visible light photocatalytic H2 production. Int. J. Energy Res.;

40:1280–1286 (2016).

3. C. Wanga, Yanhui A, P. Wang, S. Zhang, J. Qian, J. Hou, A simple method for large-scale preparation of ZnS nanoribbon film and its photocatalytic activity for dye degradation. Applied Surface Science 256, 4125-4128 (2010).
4. N. Li a, B. Zhou, P. Guo, J.Zhou, D. Jing, Int.J. of Hydrogen energy 38, 11268-11277 (2013).
5. S. N. Garaje, S. K. Apte, S. D. Naik, J. D. Ambekar, R.S. Sonawane, M.V. Kulkarni, A.Vinu, and B. B. Kale, Novel template-free, large scale synthesis of nanostructured CdxZn1-xS with tuneable band structure for H2 production and organic dye degradation using solar light, J. Environmental Science & Technology.
6. E. A. Kozlovaa, Yu. Kurenkovaa, A. Kolinkoa, A. Saraeva, E. Yu. Gerasimova, and D. V. Kozlova, Photocatalytic Hydrogen Production Using Me/Cd0.3Zn0.7S (Me = Au, Pt, Pd) Catalysts: Transformation of the Metallic Catalyst under the Action of the Reaction Medium, Kinetics and Catalysis.86, 431–440.
7. Dina V. Markovskaya, Ekaterina A. Kozlova, Olga A. Stonkus,
Andrey A. Saraev, Svetlana V. Cherepanova, Valentin N. Parmon, Int. J.Hydrogen energy 42, 30067 -30075 (2017).
8. Xin Xu, Ruijuan Lu, Xiaofei Zhao, Sailong Xu, Xiaodong Lei, Fazhi Zhang∗, David G. Evans, Fabrication and photocatalytic performance of a ZnxCd1−xS solid solution prepared by sulfuration of a single layered double hydroxide precursor. Applied Catalysis B: Environmental 102, 147-156 (2011).
9. Xing C, Y. Zhang, W. Yan, and L. Guo, Band structure-controlled solid solution of Cd1-xZnxS photocatalyst for hydrogen production by water splitting. International Journal of Hydrogen Energy. 31(2006): 2018-2024.
10. S. Zu, Z. Wang, Bo Liu, X. Fan, G. Qian, Synthesis of nano-CdxZn1−xS by precipitate-hydrothermal method and its photocatalytic activities. J. Journal of Alloys and Compounds 476, 689–692 (2009).
11. X. Maa, Q. Jianga, W. Guob, M. Zhenga, W. Xua, F. Maa, B. Hou. Fabrication of g-C3N4/Au/CdZnS Z-scheme Photocatalytic to Enhanced Photocatalysis Performance. J.RSC advance 1-3 (2013).
12. J. Mohapatra, Defect-related blue emission from ultra-fine Zn1−xCdxS quantum dots synthesized by simple beaker chemistry.J. International Nano Letters 2013 3:31 (2013).
13. N. Soltani, A. Dehzangi, A. Kharazmi, E. Saion, W.M.M. Yunus, B.Y. Majlis, M.R. Zare, E. Gharibshahi, and N. Khalilzadeh, Structural, optical and electrical properties of zns nanoparticles affecting by organic coating. Chalcogenide Letters. 11,79-90, (2014).
14. J. Mohapatra, Defect-related blue emission from ultra-fine Zn1−xCdxS quantum dots synthesized by simple beaker chemistry.J. International Nano Letters 2013 3:31 (2013).
15. I. Devadoss, P. Sakthivel, S. Muthukumaran, N. Sudhakar, Enhanced Blue-light emission on Cd0.9-xZn0.1CrxS($0 \leq x \leq 0.05$) quantum dots.J. Ceramics International(2018).
16. P. Sakthivel, T. Jayasri, J. Madhumitha, S. Mahalakshmi, N. Subhashini, Influence of Cd on optical and photoluminescence behavior of Zn0.98-xCdxMn0.02S quantum dots under Ar atmosphere. J.

Optik 154 74-82 (2018).

17. I. Devadoss 1, S. Muthukumarann, Band gap tailoring and yellow band emission of Cd0.9xMnxZn0.1S (x¼0 to0.05) nanoparticles: Influence of Mn concentration. J. Materials Science in Semiconductor Processing 41, 282-290 (2016).
18. H. Wang, Y. Li, D. Shu, X. Chen, X. Liu, X. Wang, J. Zhang and H. Wang, CoPtx-loaded Zn0.5Cd0.5S nanocomposites for enhanced visible light photocatalytic H2 production. Int. J. Energy Res.; 40:1280–1286 (2016).
19. X. Xu, R. Lu, X. Zhao, S. Xu, X. Lei, F. Zhangs, David G. Evans, Fabrication and photocatalytic performance of a ZnxCd1−xS solid solution prepared by sulfuration of a single layered double hydroxide precursor. J. Applied Catalysis B: Environmental 102, 147-156 (2011).
20. B. Khamala, L. Franklin, Y. Malozovsky a, A. Stewart, H. Saleem, D. Bagayoko, Calculated electronic, transport, and bulk properties of zinc-blende zinc sulphide (zb-ZnS). J. Computational Condensed Matter6, 18-23, (2016).
21. S. Joishy, A. Antony, P. Poornesh, R.J. Choudhary, B. Rajendra, Influence of Cd on Structure, Surface Morphology, Optical and Electrical Properties of Nano Crystalline ZnS Films. J. Sensors and Actuators: A. Physical, S0924-4247(19)31684-X (2019).
22. M. Askari, N. Soltani, E. Saion, W. Mahmood Mat Yunus, H. Maryam Erfani, M. Dorostkar, Structural and optical properties of PVP-capped nanocrystalline ZnxCd1-xS solid solutions. J. Superlattices and Microstructures S0749-6036(15)00032-4 (2015).

Table

Table 1. Calculated crystalline parameters of $Cd_{1-x}Zn_xS$ nanocompounds and Au/$Cd_{1-x}Zn_xS$ nanocomposites

Catalyst Composition	Peak position	FWHM(b) (°)	d-spacing (A°) (111)	Lattice parameter a = b = c(Å)	Crystallite Size (nm)
CdS	26.479	3.51683	3.336	5.76	2.349
$Cd_{0.75}Zn_{0.25}S$	26.995	4.25919	3.304	5.71	1.927
$Cd_{0.5}Zn_{0.5}S$	27.123	6.96636	3.280	5.68	1.178
$Cd_{0.25}Zn_{0.75}S$	28.285	2.98645	3.152	5.45	2.772
ZnS	28.757	2.7623	3.10	5.36	2.961
Au/CdS	26.564	5.68563	3.352	5.80	1.43
$Au/Cd_{0.75}Zn_{0.25}S$	26.823	5.45261	3.321	5.75	1.497
$Au/Cd_{0.5}Zn_{0.5}S$	26.823	5.45261	3.321	5.69	1.493
$Au/Cd_{0.25}Zn_{0.75}S$	28.069	6.63232	3.176	5.49	1.23
Au/ZnS	28.499	2.75013	3.129	5.40	2.98

Figures

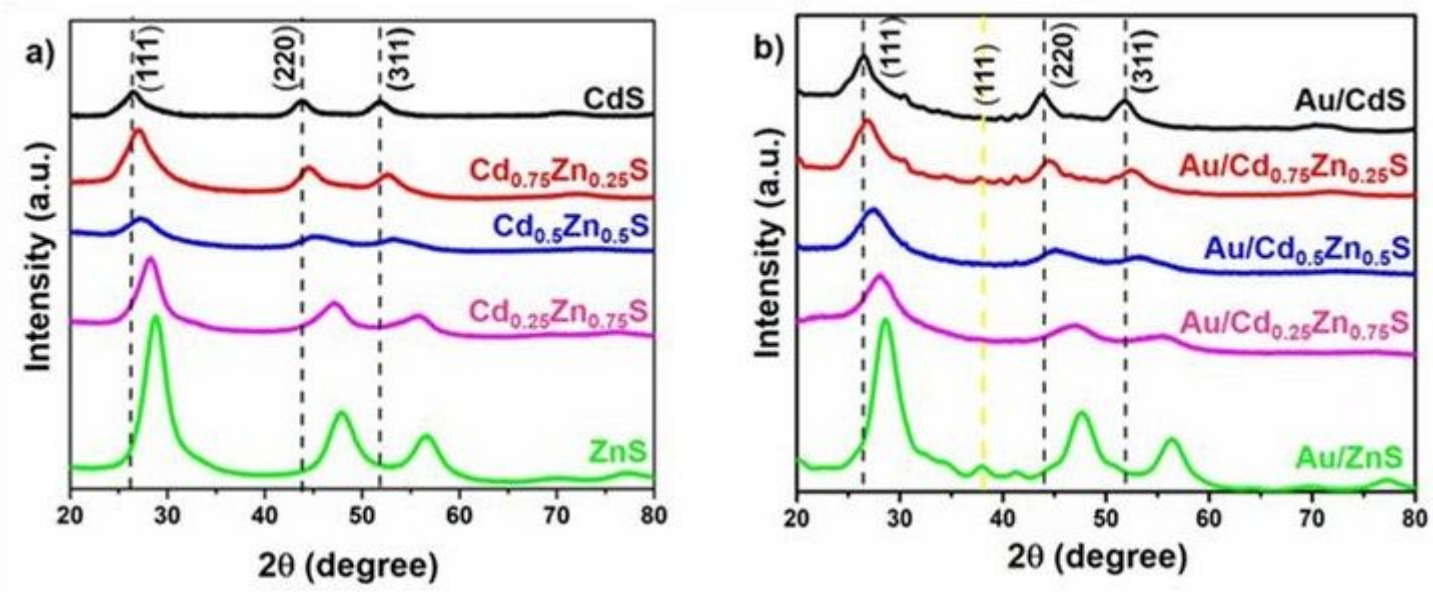

Figure 1

a). XRD patterns of Cd1-xZnxS nanocompounds and b) Au/Cd1-xZnxS nanocomposites

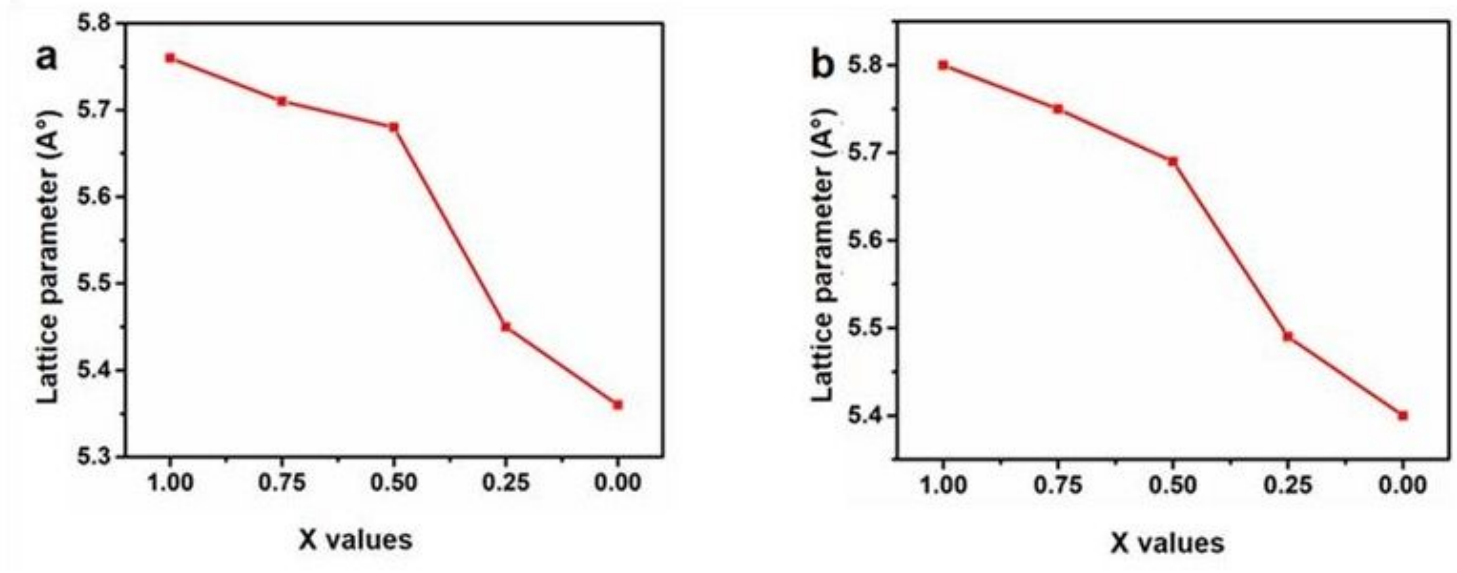

Figure 2

a). The lattice constant values of Cd1-xZnxS nanocompounds and b) Au/Cd1-xZnxS nanocomposites for different Zn values obtained from XRD patterns.

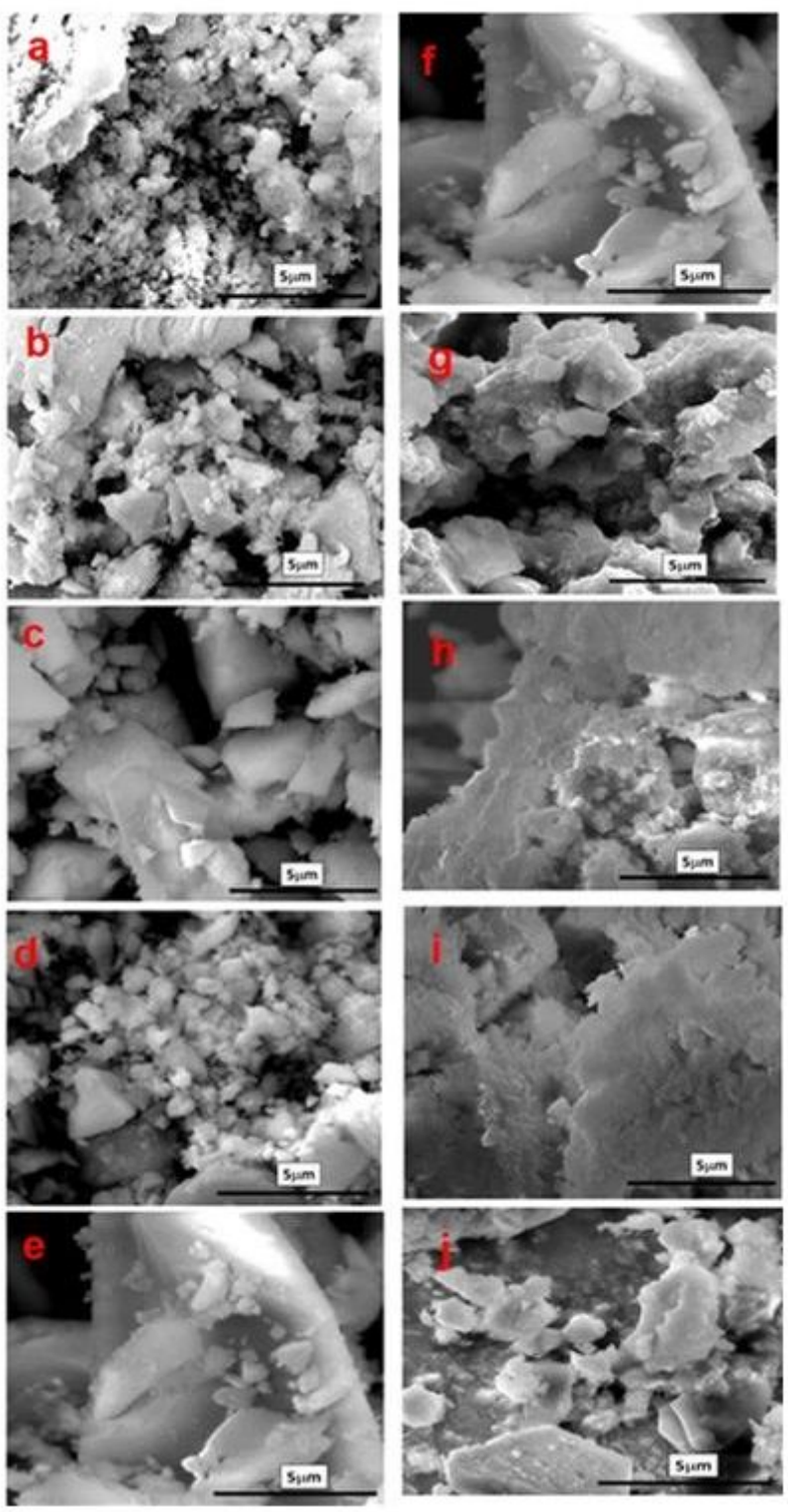

Figure 3

(a-e) SEM images of Cd1-xZnxS nanocompounds and (f-j) Au/Cd1-xZnxS nanocomposites

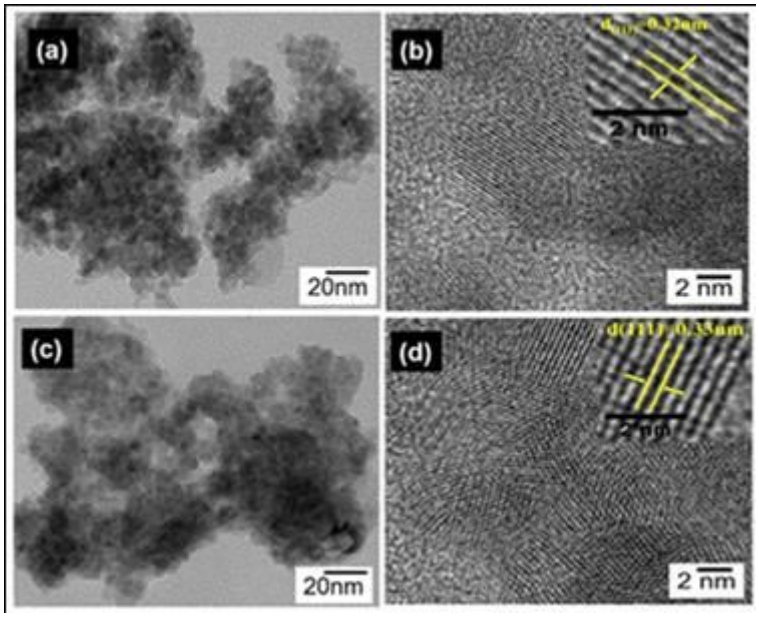

Figure 4

HRTEM images of Cd0.25Zn0.75S nanocompound (a&b) and Au/Cd0.25Zn0.75S nanocomposite (c&d).

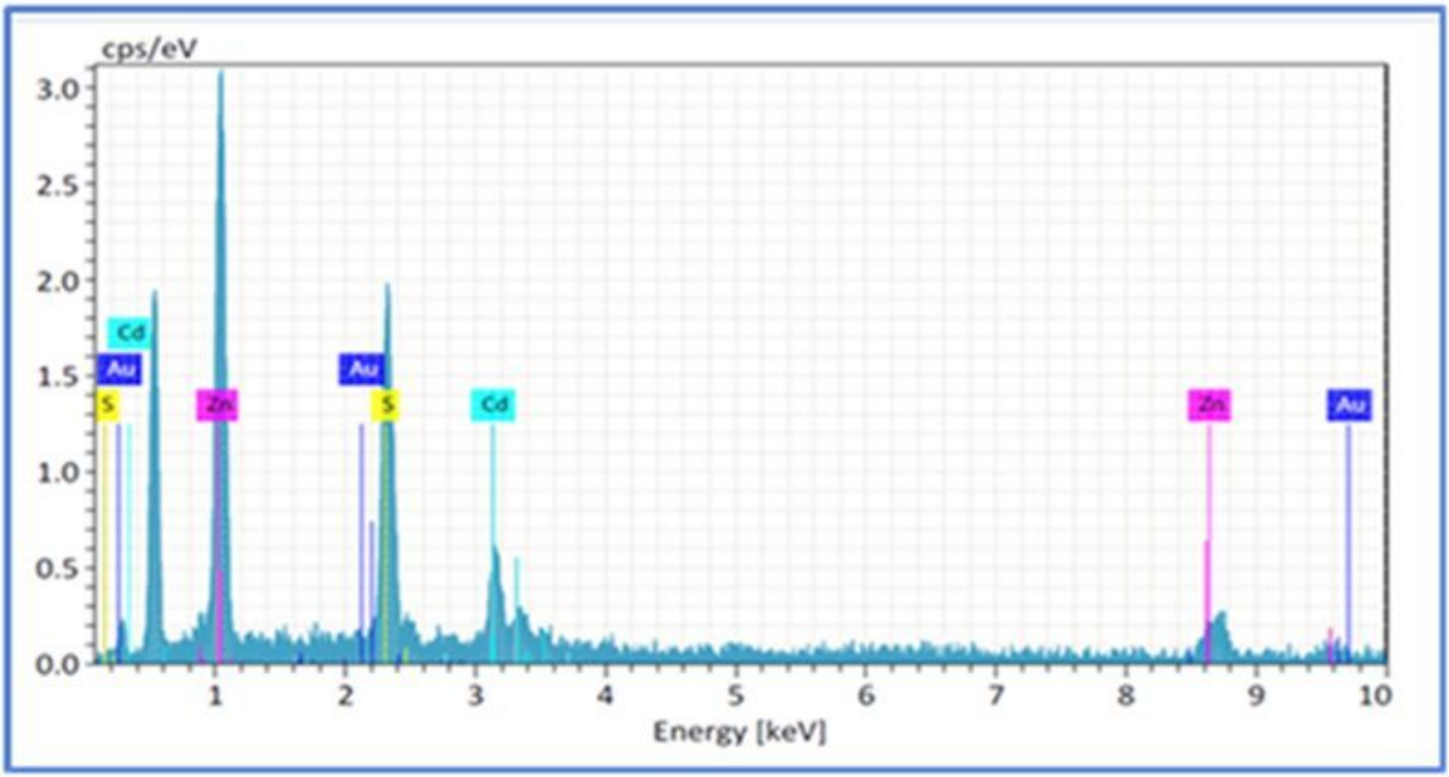

Figure 5

EDX spectrum of Au/Cd0.25Zn0.75S nanocomposite

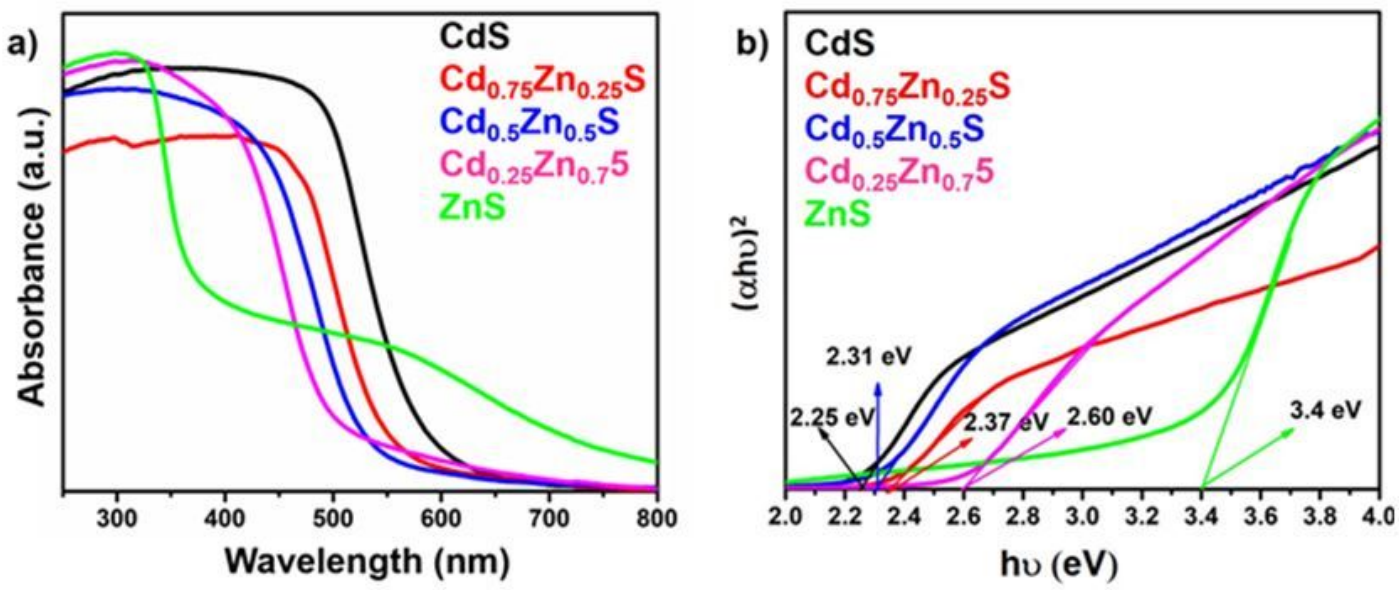

Figure 6

Optical absorption spectrum of Cd1-xZnxS nanocompounds (a) and their correspondingTauc's plots (b).

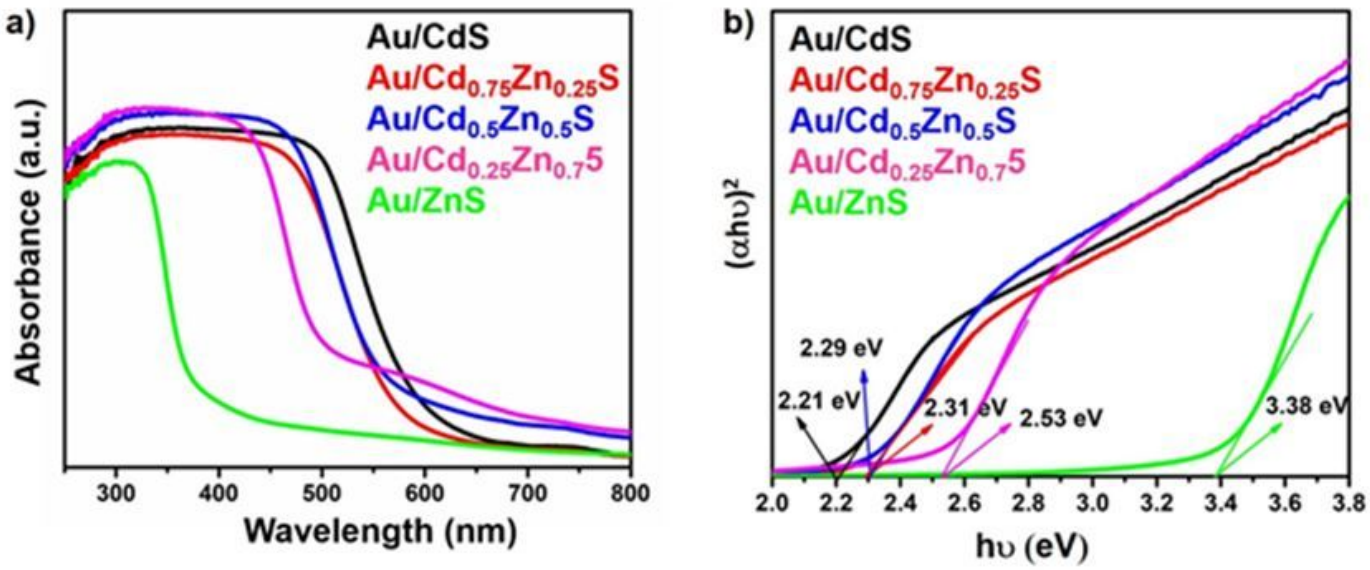

Figure 7

Optical absorption spectrum of Au/Cd1-xZnxS nanocomposites (a) and their corresponding Tauc's plots (b).

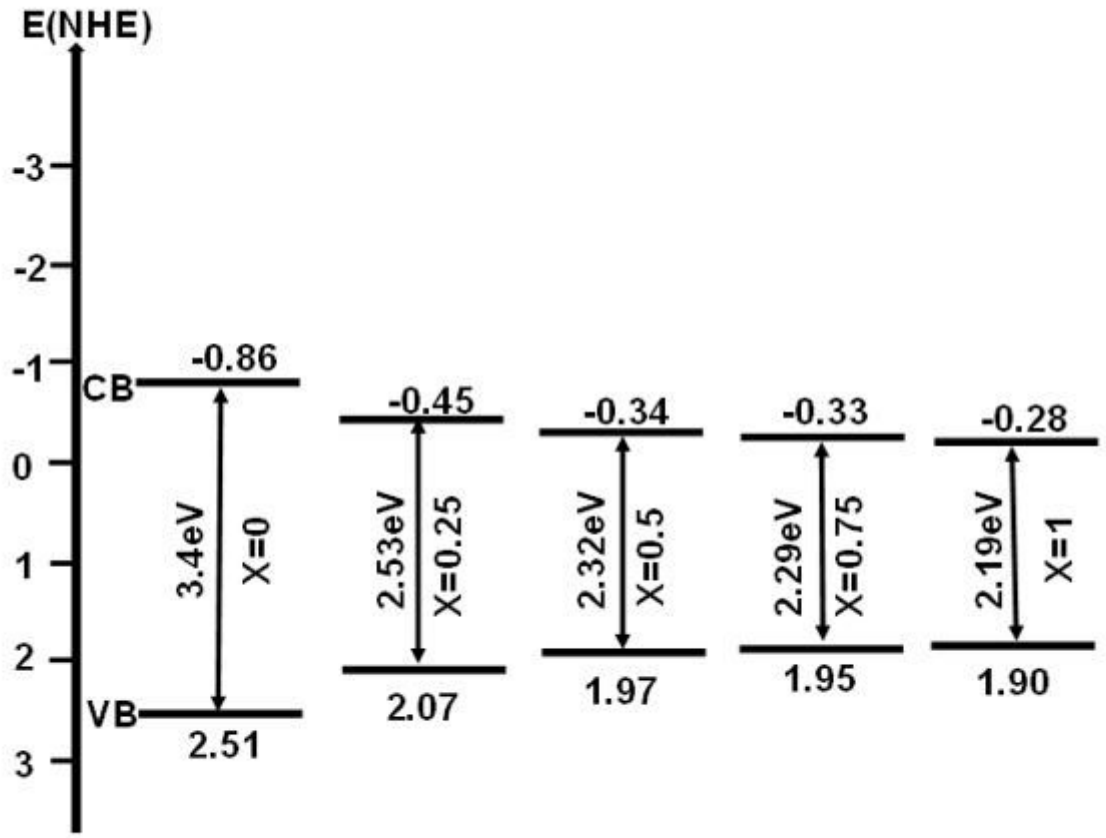

Figure 8

Energy band diagram of Cd1-xZnxS nanocompounds

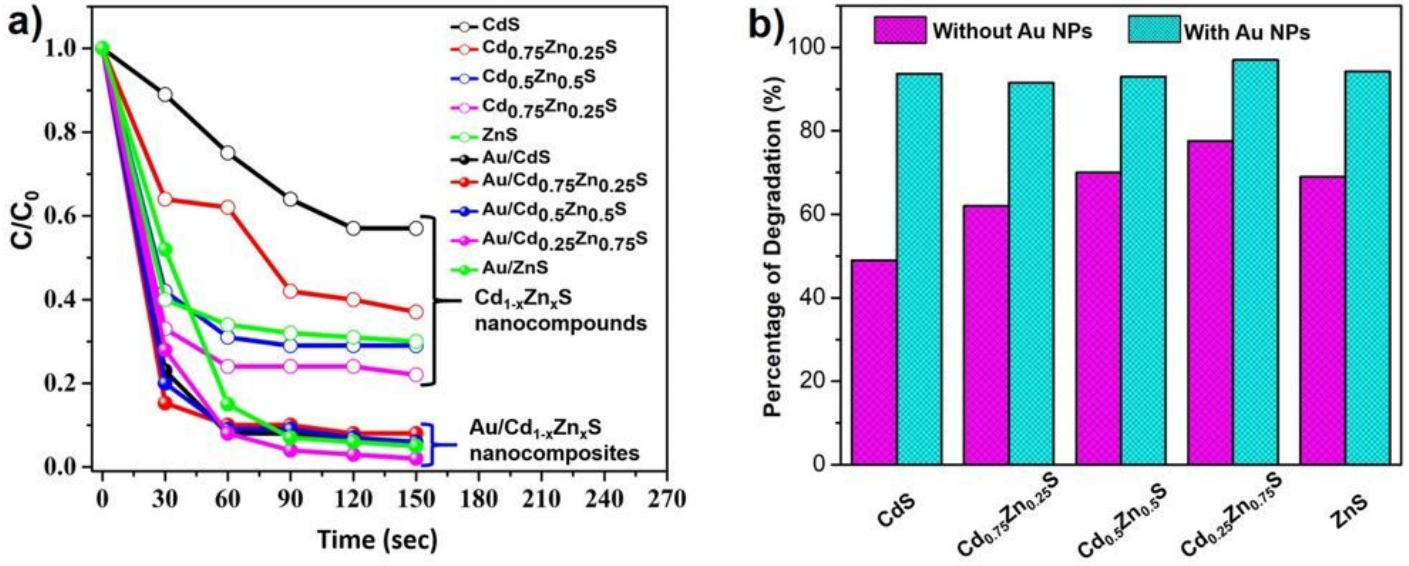

Figure 9

a). C/C0 versus Time graph of the photocatalytic degradation reactions of the various catralysts (b) Photocatalytic percentage of efficiency of the nanocatalysts

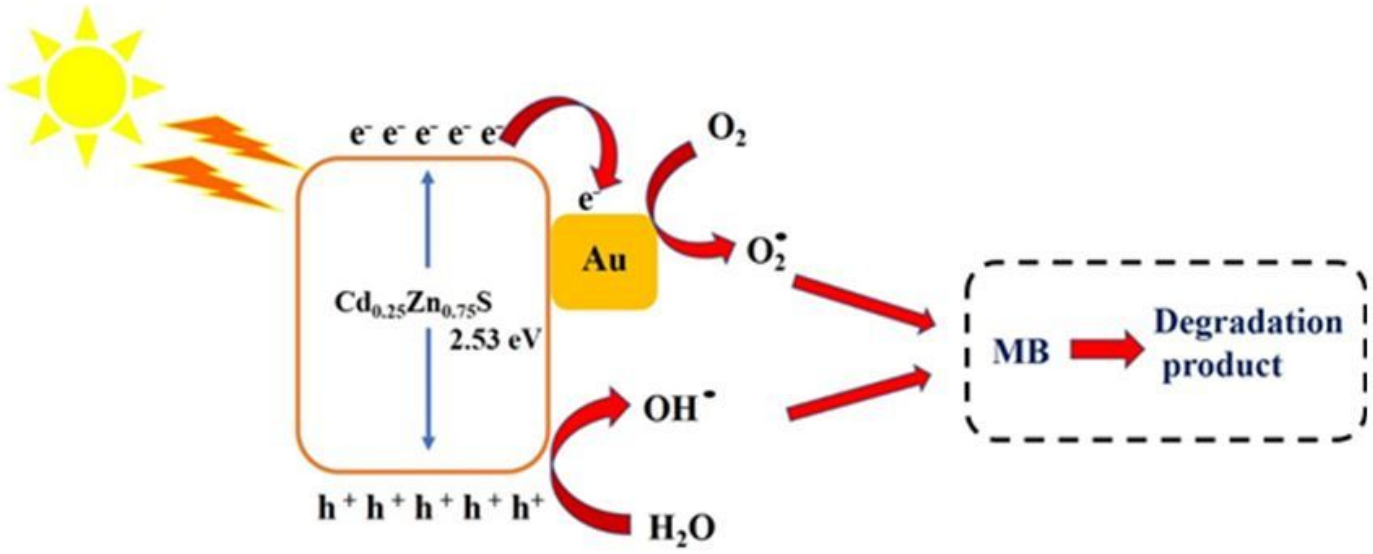

Figure 10

Charge transfer mechanism of Au incorporated CdZnS nanocompounds